

## GLIMMERITE XENOLITHS IN EARLY PROTEROZOIC ULTRAPOTASSIC ROCKS FROM THE CHURCHILL PROVINCE\*

TONY D. PETERSON AND ANTHONY N. LeCHEMINANT

*Geological Survey of Canada, 601 Booth Street, Ottawa, Ontario K1A 0E8*

### ABSTRACT

Phlogopite-rich xenoliths ( $\leq 3$  cm in diameter) occur in ultrapotassic feeder dykes and flows of the Christopher Island Formation (ca. 1.84 Ga) throughout a  $600 \times 300$  km area in the central Churchill Province in the District of Keewatin. The glimmerite xenoliths are subspherical to prolate, with smooth and well-rounded surfaces. Most have a concentric rind of distorted and recrystallized phlogopite that is interpreted to result from collisions with the conduit walls during magma ascent. Mineral inclusions in the rinds are typically flattened and boudinaged. The core of the xenoliths is dominated by coarse-grained phlogopite and carbonate minerals with igneous textures. Minor phases in the core and rind are calcite, dolomite, strontianite, chromite, chromian diopside, Al-poor amphibole, titanite, zircon, apatite, rutile, sulfides, epidote, barite, goethite, quartz, and fluorite. Phlogopite from xenoliths [average  $\text{Cr}_2\text{O}_3$  1.2 wt%,  $\text{TiO}_2$  0.7 wt%, atomic  $\text{Mg}/(\text{Mg}+\text{Fe}_T)$  0.92] is more primitive than that occurring as phenocrysts in the host magma [average  $\text{Cr}_2\text{O}_3$  0.1 wt%,  $\text{TiO}_2$  2.5 wt%,  $\text{Mg}/(\text{Mg}+\text{Fe}_T)$  0.82]. The xenoliths resemble MARID (Mica – Amphibole – Rutile – Ilmenite – Diopside) xenoliths found in kimberlites, but are relatively depleted in Ti-bearing phases. The glimmerite xenoliths are interpreted to be fragments of mantle pegmatites and wall-rock cumulates, formed by solidification of primitive ultrapotassic melts with phlogopite  $\pm$  magnésiochromite  $\pm$  chromian diopside on the liquidus, and carbonate minerals  $\pm$  a silica polymorph crystallizing near the solidus.

*Keywords:* Churchill Province, lamproïte, lamprophyre, minette, phlogopite, Proterozoic, ultrapotassic, xenoliths, District of Keewatin.

### SOMMAIRE

Des xénolithes riches en phlogopite, ayant un diamètre de trois cm ou moins, sont répandus sur une superficie de  $600 \times 300$  km dans des filons nourriciers et des coulées ultrapotassiques de la formation de Christopher Island (environ 1.84 Ga), dans la partie centrale de la province de Churchill, district de Keewatin. Ces xénolithes de glimmerite ont une forme subsphérique à allongée, et possèdent une surface lisse et arrondie. La plupart montrent un liseré de phlogopite déformé et recristallisé qui résulterait des multiples collisions avec les parois lors de la montée du magma. Les inclusions minérales de ces liserés sont typiquement aplaties ou en forme de boudin. Le cœur des xénolithes contient surtout phlogopite et carbonates ayant une texture ignée. Parmi les phases mineures dans le cœur et les liserés figurent calcite, dolomite, strontianite, chromite, diopside chromifère, amphibole sub-alumineuse, titanite, zircon, apatite, rutile, sulfures, épidote, baryte, goethite, quartz et fluorite. La phlogopite des xénolithes [teneur moyenne en  $\text{Cr}_2\text{O}_3$ , 1.2% en poids, et en  $\text{TiO}_2$ , 0.7%; rapport molaire  $\text{Mg}/(\text{Mg} + \text{Fe}_T) = 0.92$ ] est plus primitive que celle des phénocristaux du magma hôte [teneur moyenne en  $\text{Cr}_2\text{O}_3$ , 0.1% en poids; et en  $\text{TiO}_2$ , 2.5%; rapport molaire  $\text{Mg}/(\text{Mg} + \text{Fe}_T) = 0.82$ ]. Ces xénolithes ressemblent aux xénolithes MARID (Mica – Amphibole – Rutile – Ilménite – Diopside) typiques des kimberlites, mais ils sont relativement appauvris en minéraux titani-fères. Les xénolithes de glimmerite seraient des fragments de pegmatites du manteau et de cumulats formés le long des parois par solidification de liquides ultrapotassiques primitifs ayant, sur le liquidus, phlogopite  $\pm$  magnésiochromite  $\pm$  diopside chromifère, et, plus près du solidus, des carbonates  $\pm$  un polymorphe de silice.

(Traduit par la Rédaction)

*Mots-clés:* lamproïte, lamprophyre, minette, phlogopite, protérozoïque, ultrapotassique, xénolithes, province de Churchill, district de Keewatin.

\* Geological Survey of Canada contribution 18992.

## INTRODUCTION

Voluminous and widespread ultrapotassic magmatism occurred within the District of Keewatin (central Churchill Province) during the latter stages of the Trans-Hudson orogeny, at approximately 1.84 Ga (Tella *et al.* 1985, Peterson, unpubl. data). The volcanic rocks are interbedded with fluvial, lacustrine, and alluvial fan deposits (Christopher Island Formation, CIF) in fault-bounded basins containing sequences up to 2.5 km thick (Fig. 1). The CIF is considered to be a syn- to postcollisional suite, with eruption triggered by intracratonic deformation within the Churchill Province due to continental collisions on the margins of Laurentia (Hoffman 1980, LeCheminant *et al.* 1987, Hoffman & Peterson 1991).

Volcanic flows of the CIF, and lamprophyric feeder dykes, have mineral assemblages typical of minettes and some lamproites (Blake 1980, LeCheminant *et al.* 1987, Peterson 1992). Rocks with a  $mg\# \geq 60$  [ $mg\# = 100Mg/(Mg+Fe_{T})$ ] contain phenocrysts of apatite, phlogopite, clinopyroxene, magnetite, and altered

leucite (rare), with altered olivine in about 25% of the samples. The groundmass always contains K-feldspar, with variable amounts of phlogopite, clinopyroxene, magnetite, titanite, Al-poor alkali amphiboles, calcite, rutile, and quartz.

The igneous rocks of the CIF were classified as transitional from minettes to lamproites by Peterson (1992). Subsequent detailed geochemical comparison to other ultrapotassic suites (Peterson *et al.* 1993) has shown that many high- $mg\#$  (and several low- $mg\#$ ) samples most closely resemble lamproites. Other samples resemble minette-like and lamproitic rocks of uncertain affinity, such as those of the Gondwana coalfields, India (Scott Smith 1989) and of Spain (Venturelli *et al.* 1991). Also included in the suite are rare weakly potassic to sodic trachytes, which are presumed to represent fractionated and crustally contaminated, mafic potassic magmas. The CIF lamproites differ from the average lamproite of Bergman (1987) in having slightly higher  $Al_2O_3$  and  $Na_2O$  contents, and strong relative depletions in high-field-strength elements, particularly Ti and Zr. Since the overall

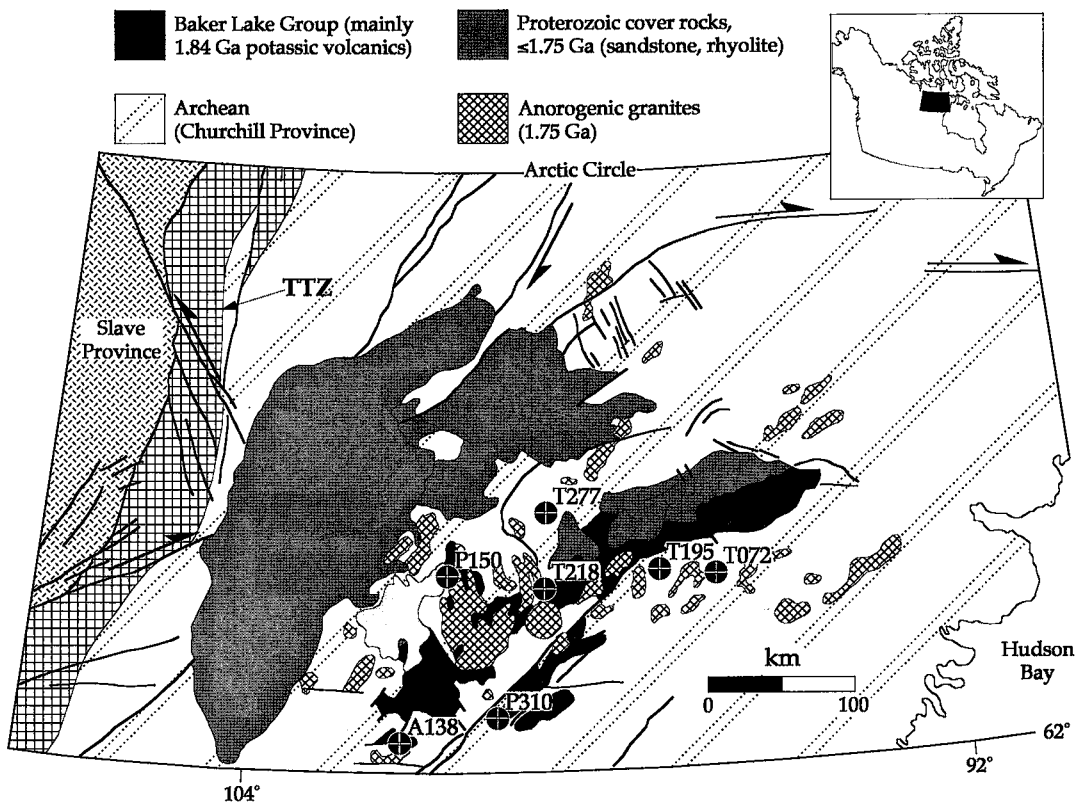


FIG. 1. Simplified geology of the Keewatin Hinterland, and locations of samples discussed in this paper. TTZ: Thelon Tectonic Zone (2.1–2.0 Ga suture between Slave and Churchill cratons). Sample P92/213B is from the same location as P310.

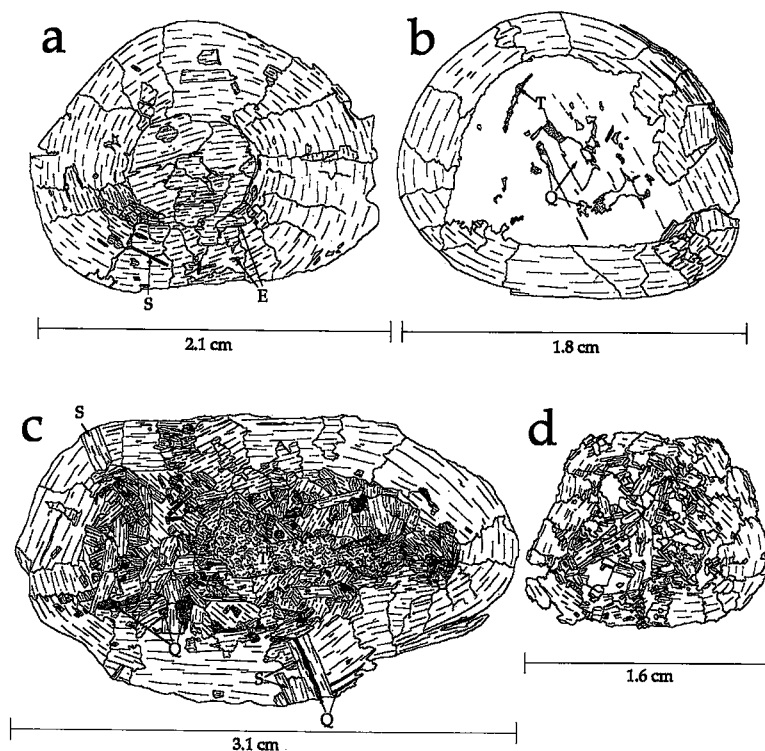


FIG. 2. Traces of thin sections of glimmerite xenoliths. a. T218-X3. b. T277-X1. c. T277-X2. d. T277-X3. Xenoliths T218-X3 and T277-X3 are not discussed in the text but have mineral assemblages identical to those in T218-X and T277-X2, respectively. Symbols: E epidote, Q quartz, S secondary phlogopite, T talc.

character of the CIF (particularly the highest mg# samples) is lamproitic, for simplicity we will refer to all samples discussed in this paper as lamproites.

Peridotitic or eclogitic xenoliths have not been found in dykes or flows of the CIF, although crustal xenoliths are locally abundant. However, unusual ellipsoidal phlogopitite ("glimmerite") xenoliths occur in several phlogopite diopside ( $\pm$  olivine  $\pm$  magnetite) lamproite flows and dykes, which invariably have a mg# greater than 60. Approximately 100 xenoliths have been collected from nine localities. They consist of a phlogopite- and calcite-rich core jacketed by a rind of concentric phlogopite with [001] cleavage planes parallel or subparallel to the xenolith surface (Fig. 2). Mineral compositions are dissimilar to those of the associated phenocrysts, and the glimmerite xenoliths cannot be low-pressure cognate cumulates. Coarse-grained phlogopite - diopside - magnetite xenoliths, which occur in many samples, are interpreted as low-pressure cumulates (e.g., Fig. 7f of Peterson 1992).

Some of the glimmerite xenoliths from CIF rocks are identical to those described from a lamproite at

Oqaitsúnguít, west Greenland, by Skerjnaa (1992), dated at 1.75 Ga (K-Ar, phlogopite). Smith (1936) mentioned a similar 2-cm spherical fragment of biotite with tangentially arranged cleavage planes collected from the South Hill lamprophyre, Jersey. Phlogopite-rich xenoliths of the MARID (Mica - Amphibole - Rutile - Ilmenite - Diopside) suite, which resemble the glimmerites, occur in some kimberlites and are generally interpreted as crystallized ultrapotassic melts, such as lamproite magma (e.g., Waters 1987). As such, they may provide constraints on the composition and depth of origin of ultrapotassic magmas in the subcontinental lithosphere. In this paper, we give textural and mineralogical data on selected xenoliths of glimmerite, speculate on their origin, and discuss their significance for the petrogenesis of the CIF ultrapotassic rocks.

#### DESCRIPTION OF THE XENOLITHS

Eight xenoliths from five dykes and one flow were selected for detailed study on the basis of freshness,

TABLE 1. MINERALOGY OF SELECTED GLIMMERITE XENOLITHS

	l x w, cm	core	rind
T072-X1	1.7 x 2.5	<b>Phl, Chr, Sul, Cal, Ttn, Aam, Tr, Qtz, Chl, Brt, Ap</b>	<b>Chr, Cpx, Cal, Str, Brt, Ap, Sul, Cal/Mag, Kfs</b>
T072-X2	1.0 x 1.3	<b>Phl, Chr, Sul, Cal, Aam, Tr, Qtz, Srp, Brt</b>	<b>Chr, Cpx, Cal, Cal/Mag, Kfs</b>
T072-X3	0.4 x 0.4	<b>Aam, Brt</b>	<b>Chr, Cpx, Zrn</b>
T218-X	1.9 x 2.6	<b>Phl, Ttn, Qtz, Cal, Aam, Tr, Ep, Fl, Mag</b>	<b>Qtz, Cal, Tr, Ep, Fl, Cal/Mag</b>
T277-X1	1.6 x 1.8	<b>Phl, Cal, Qtz, Aam</b>	<b>Cal, qz, Aam, Ep, Qtz, Rt</b>
T277-X2	2.0 x 3.2	<b>Phl, Tlc, Aam</b>	<b>Cal, Qtz, Ep, Cal/Mag, Cpx, Qtz, Rt</b>
T195-X	2.0 x 3.0	<b>Phl, Cal, Qtz, Rt, Gt</b>	<b>Chr, Cal, Qtz, Ap, Brt, Rt, Dol</b>
A138-X	1.2 x 1.4	<b>Phl, Chr, Cpx, Kfs</b>	<b>Chr, Cpx, Kfs</b>

**Bold:** primary; plain: secondary (metamorphic); *italicized:* magma infiltration.

Aam=alkali amphibole, Ap=apatite, Brt=barite and other sulphates, Cal/Mag=calcite/magnetite (after epidote), Cal=calcite, Chl=chlorite, Chr=chromite, Cpx=clinopyroxene, Dol=dolomite, Ep=epidote, Fl=fluorite, Gt=goethite, Kfs=orthoclase, Phl=phlogopite, Qtz=quartz, Rt=rutile, Srp=serpentine, Str=strontianite, Sul=sulfides, Tlc=tacl, Tr=tremolitic amphibole, Ttn=titanite, Zrn=zircon. All xenoliths have phlogopite in the rind.

variety of mineral assemblage, and wide geographic distribution (locations in Fig. 1). The dykes are typically less than 5 m wide, with chilled margins showing variable alignment of phlogopite phenocrysts, and slightly coarser centers with visible K-feldspar in the groundmass. The characteristics of the selected xenoliths of glimmerite are summarized in Table 1. We will also refer to a mafic lamproite breccia, site of sample P150, which contains microxenoliths and xenocrysts derived from disaggregated xenoliths of glimmerite, and to a flow (sample P310) containing angular xenoliths of what are probably metasomatized wallrocks. Another breccia (P92/213) near the site of sample P310 contains no glimmerite fragments, but is exceptionally fresh and has yielded useful mineralogical data; both breccias are partly welded rocks containing fragments of glassy phlogopite – diopside lamproite.

The glimmerite xenoliths are subspherical to ellipsoidal, with length-to-width ratios of up to 3:2. Nearly all of the xenoliths have a complete and even rind composed of a sheet of phlogopite 0.25 – 1 cm thick (Figs. 2a – d, 3a, 4a). Bends in the rind are accommodated by kink bands, smoothly curved [001] cleavage planes, and irregular, mostly radially oriented, serrate grain-boundaries concentrated in the regions of tightest curvature. In some xenoliths, the rind is smooth, unbroken, and optically continuous; in others, it is ruptured and has irregular inner and outer surfaces. In xenoliths where the core consists of randomly oriented polycrystalline phlogopite, the rind grades continuously through a zone where phlogopite is partly oriented parallel to the rind fabric (e.g., Figs. 2c, d). Xenolith T072 – X1 is notable for having a near-perfect rind (Fig. 3a). Xenolith A138 – X has a reaction rim on its

surface, composed of euhedral magnetite and anhedral K-feldspar. No other xenolith has a reaction rim, although magmatic infiltration did occur through ruptured rinds in some cases.

Phlogopite crystals oriented at random angles to the rind fabric are common, particularly near the inner and outer surfaces of the rinds (Figs. 3b, 4b). Up to three generations of phlogopite that cross-cut one another, and incorporate pre-existing inclusions, are observed. Inclusions of calcite, rutile, quartz, amphibole, fluorite, barite, and epidote in rind phlogopite typically occur as elongate lenses and ribbons along the cleavage planes (Figs. 4a, c). Calcite inclusions may be boudinaged (Fig. 4d). Clinopyroxene occurs as irregular and partly resorbed fragments transposed along the rind fabric.

The core of the xenoliths is usually dominated by phlogopite containing inclusions of the same minerals found in the rind. In some cases, the core consists of a single crystal of phlogopite with ribbon-shaped inclusions. In appropriately oriented sections, the core phlogopite is seen to be continuous with the rind on one side of the xenolith (Fig. 2b). These single-phlogopite-cored xenoliths are identical to those described from Oqaitúnguít by Skerjnaa (1992). In some cases, the core is comprised of randomly oriented polycrystalline phlogopite (grain size  $\leq 3$  mm); these are consistently surrounded by the thinnest and most irregular rind (e.g., Fig. 2d). Xenoliths from dyke T072 have a core dominated by calcite or alkali amphibole (Figs. 3a–d, 5b–c). The calcite contains highly resorbed inclusions of phlogopite partly replaced by Ni-rich chlorite and amphibole (richterite – tremolite – winchite solid solutions).

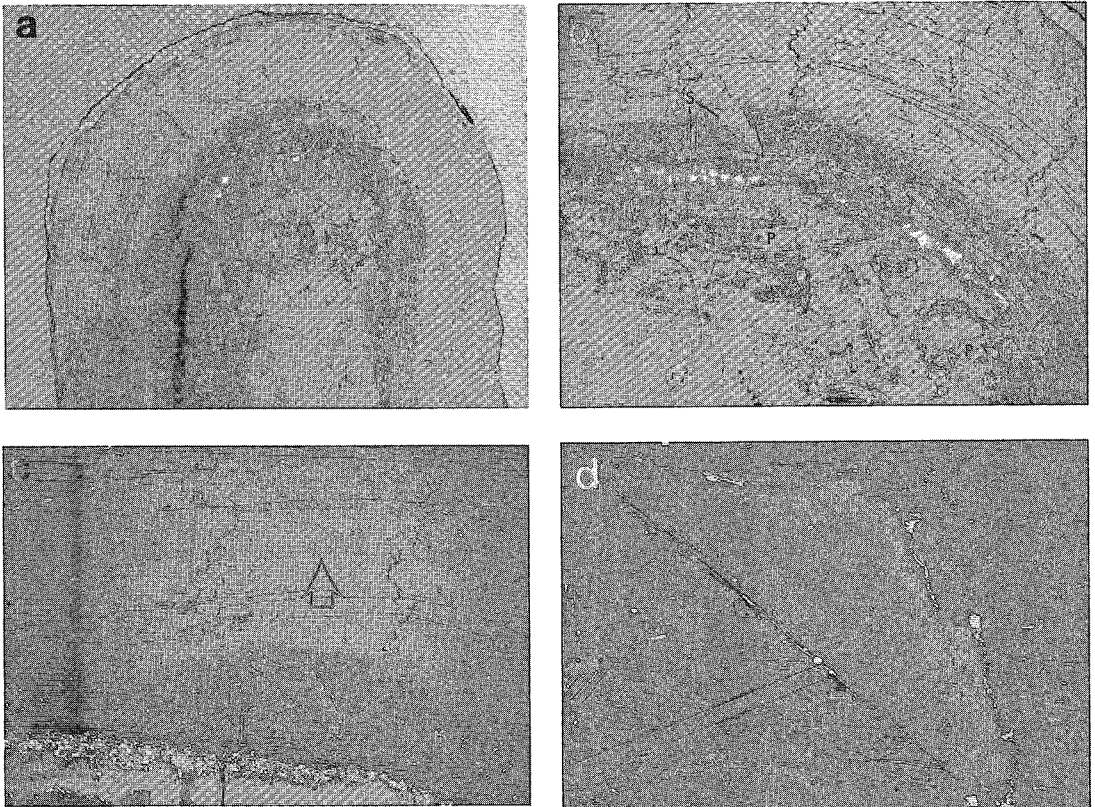


FIG. 3. Details of xenolith T072-X1. Width of field of view in parentheses. a. Photomicrograph, plane-polarized light. Note the excellent continuity of the rind, and the altered inner rind adjacent to the carbonate core, which contains highly resorbed remnants of phlogopite. The xenolith is 1.7 cm wide and 2.5 cm long; the photograph was cropped above a break in the thin section. b. Core-rind boundary, plane-polarized light. Area is the top left corner of Fig. 3a, rotated clockwise 90°. Note the highly resorbed core phlogopite (P) in carbonate, and the alteration front within the inner rind, which contains abundant small grains of secondary phlogopite (S) at a high angle to the rind fabric. Opaque minerals in band surrounding core are sulfides (1 cm). c. Back-scattered electron image of the inner portion of the rind of T072-X1. The bright mass at the outer edge of the core is rich in barite and sulfides. Note the sharp, but subtle compositional break (arrow) and the diffuse boundary of the dark (Mg-rich) inner rind. The lightest portion of the rind is richer in Fe than the inner rind, and slightly poorer in Cr than the zone above the arrow. White flecks are chromite and Fe-Ni sulfides (0.5 cm). d. Detail of the inner rind (back-scattered electron image) showing secondary phlogopite with Fe-depleted rim (dark) laced with chromite and sulfides (white). Note the tiny, bright inclusions of chromite in the primary phlogopite (1 mm).

#### MINERALOGY

The glimmerite xenoliths are mineralogically similar to MARID suite xenoliths (Dawson 1987) but are relatively depleted in Ti-bearing phases. The xenoliths broadly fall into two groups. Chromite-bearing xenoliths contain one or more of the following: chromian diopside, calcite, sulfides (pyrrhotite + pentlandite + galena), tremolitic and alkali amphibole, and zircon (xenoliths A138-X, T195-X, and those from dyke T072). Those not bearing chromite may contain magnetite, epidote, fluorite, and amphibole; calcite is rare or absent (xenoliths T218-X, T277-X1, T277-X2).

Quartz occurs in most samples, but is most abundant in chromite-absent xenoliths.

Electron-microprobe analyses (Tables 2 to 6) were obtained with a Cameca Camebax instrument using PAP software and natural minerals for standards (pure metals were used as standards for Ni and Zn). Standard conditions were: accelerating voltage 15 kV, beam current 30 nA, counting period 20 seconds; hydrous silicates were analyzed for F, Na, Mg, Al and Si with a beam current of 10 nA. Chromite was analyzed at 20 kV, with 10-second counting periods. Results of analyses are quoted in weight percent unless otherwise indicated.

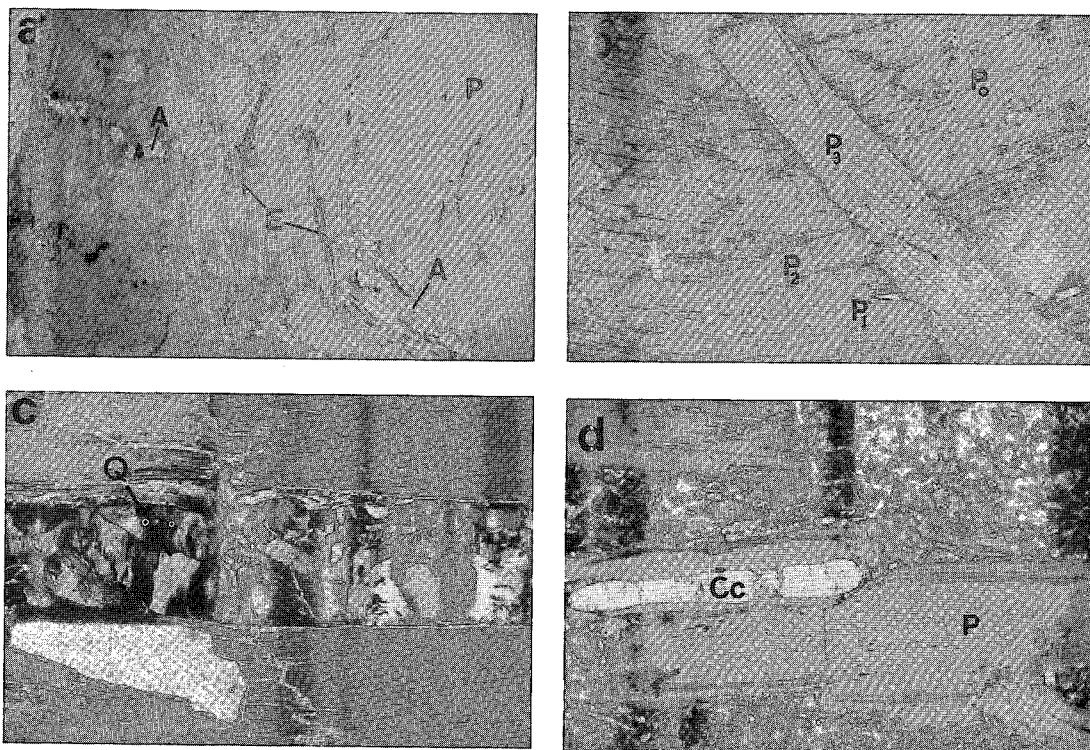


FIG. 4. Textures in xenolith rinds. Symbols: A amphibole, Cc calcite, E epidote, P phlogopite, Q quartz. Width of field of view in parentheses. a. Boundary between rind and core in T218-X. Note that epidote occurs in arcuate ribbons parallel to phlogopite cleavage, whereas amphibole grains may cross-cut the cleavage. Coarse amphibole is concentrated at the core-rind boundary. The section is cut parallel to [001] of the core phlogopite grain, which contains trains of magnetite. Opaque bodies in the rind are magnetite + calcite after epidote (7 mm). b. Secondary phlogopite in the rind of T195-X. There are three generations of phlogopite ( $P_1$ ,  $P_2$ ,  $P_3$ ;  $P_0$  is the curved phlogopite of the rind) that formed by recrystallization of the rind. Dark lines across  $P_0$  are scratches (7 mm). c. Quartz ribbon in phlogopite, T277-X2. The optical orientation of the quartz grains indicates growth, or recrystallization, in an extending fracture between cleavage planes of phlogopite. Crossed polars (0.4 mm). d. Boudinaged calcite ribbon in a phlogopite xenocryst from dyke PHA-89-K146 (sample location near P150). Opaque blades (top left) are oxidized epidote (3 mm).

### Phlogopite

Phlogopite phenocrysts in the CIF lamproites are relatively Al-rich and Ti-poor compared to those of most other lamproites (Table 2, Fig. 6). Although they overlap the low-Al end of the "minette" field of Mitchell & Bergman (1991), this portion of the field is defined by very few data-points, and is probably appropriate for transitional rocks. With decreasing  $Mg/(Mg+Fe)$ , Ti increases, Cr and Ni decrease, and Al decreases. Low-Al, high-Ti micas can display poly-synthetic twinning and pleochroism in shades of yellow-brown and orange-pink. High-(Fe, Ti, Al, Ba) phlogopite xenocrysts occur in some dykes (LeCheminant *et al.* 1987). They plot at one end of the "minette phlogopite" field of Mitchell & Bergman (1991) (Fig. 6) and probably crystallized from frac-

tionated magma, but do not appear to be part of the normal trend of mica compositions for the CIF rocks, which parallels the trends observed in lamproites.

Phlogopite in the xenoliths has normal pleochroism, with X pale golden brown, Y = Z reddish orange (Table 2). Relative to the phenocrysts (Figs. 7a - c), the phlogopite in the xenoliths is rich in Mg [ $0.85 < Mg/(Mg+Fe) < 0.97$ , except T072-X3] and Cr ( $\geq 0.5\%$   $Cr_2O_3$ ) and has low Ti (usually  $< 1\%$   $TiO_2$ ), Al (7-14%  $Al_2O_3$ ) and F ( $< 1\%$ ). The mica in the glimmerite xenoliths has higher Al, Cr, Ni, and average mg# than mica in MARID xenoliths as described by Dawson (1987), but most compositions plot within the Al-Ti MARID box of Mitchell & Bergman (1991) (Fig. 6).

No consistent variation in phlogopite pleochroism or composition from xenolith core to rim is observed,

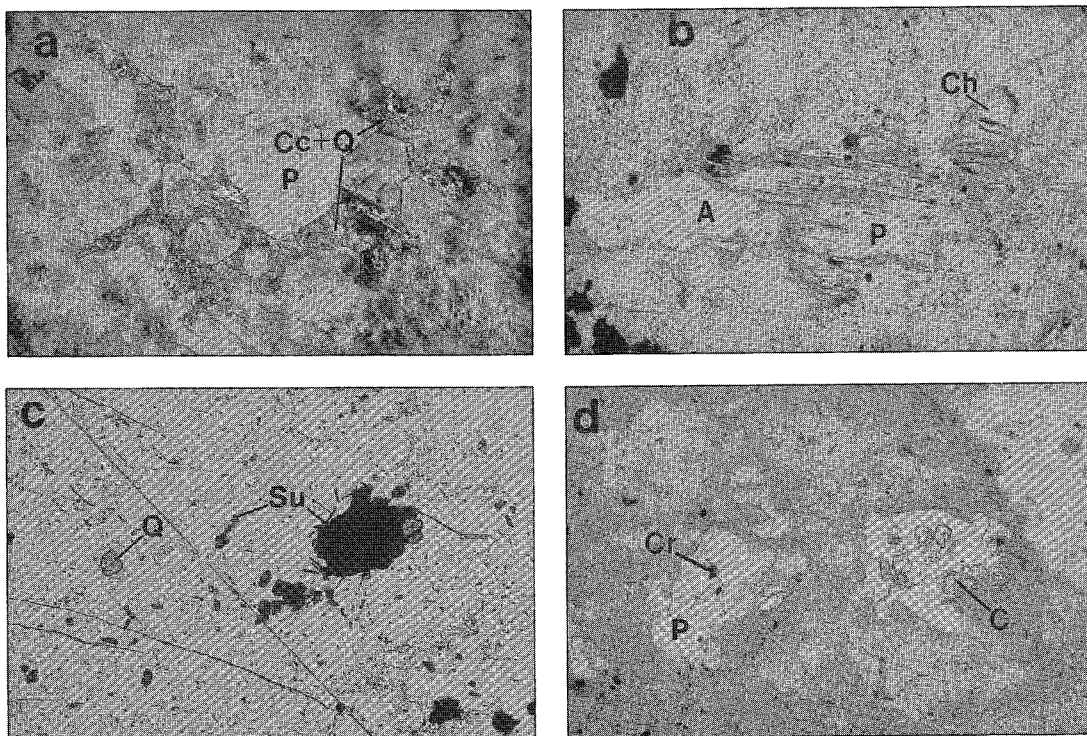


FIG. 5. Textures in xenolith cores. Symbols as in Fig. 4 and, in addition, Cr chromite, Ch chlorite, Su sulfides. a. Interstitial calcite + quartz in textural equilibrium with phlogopite, T195-X. Dark patches in phlogopite are exsolved needles of rutile (3 mm). b. Phlogopite partially replaced by richteritic amphibole and high-Ni chlorite, T072-X1 (0.4 mm). c. Sulfide and high-silica blebs (Q) in carbonate, T072-X1 (0.7 mm). d. Sieve-textured phlogopite with inclusions of chromite and chromian diopside, A138-X. The fine-textured material is phlogopite + magnetite + alkali feldspar, interpreted as a quenched, low-pressure partial melt phase. Note sieve-texture in large grain of phlogopite, top right (1 mm).

except in T072 xenoliths (Table 3). For example, in T195 - X, phlogopite in the core and rind, and secondary phlogopite cross-cutting the rind, all have identical compositions. Xenolith T072 - X1 contains a compositional break in the inner rind. A zone of very high-mg# phlogopite 1.5 mm thick surrounds the core, and has a diffuse outer margin deflected by grain boundaries. This zone is rich in small ( $\leq 0.5$  mm) grains of phlogopite oriented at random angles to the rind fabric, and needles of chromite and irregular grains of sulfides. A phlogopite grain (Fig. 3d) within the high-Mg zone has a high-Mg core, a thin outer zone slightly enriched in Ba, and an (Fe,Ti,Cr)-depleted rim laced with chromite, pyrrhotite, and pentlandite. The remainder of the rind contains optically sharp but faint boundaries subparallel to the rind fabric, separating domains with variable Cr content but near-constant mg#.

In xenoliths T072 - X1 and T072 - X2, the core phlogopite has a highly variable composition, including some exceptionally (Al,Cr)-poor and relatively Fe-

rich domains. Phlogopite adjacent to and included in core calcite is resorbed and partly replaced by Ni-rich chlorite, barite, and quartz. Secondary (metamorphic) amphibole has overgrown both phlogopite and chlorite. Euhedral grains of chromite strongly zoned to a Fe-rich rim are included in the phlogopite. The core phlogopite trends toward Ti-poor "tetraferriphlogopite", similar to microphenocrysts in micaceous kimberlites (orangeites) (Mitchell & Bergman 1991); this trend was not noted in the other xenoliths. However, late phlogopite that nucleated on the surface of carbonate grains in the groundmass of one flow (Table 2, anal. 9) has a similar composition.

Numerous xenoliths of glimmerite have a core consisting of fibrous talc with minor quartz  $\pm$  amphibole  $\pm$  dolomite. The talc is clearly secondary but contains no relict Al-poor, Mg-rich silicate minerals; however, relict phlogopite is usually present. In xenolith A138 - X, segregations of fine-grained, brown-green mica with minor magnetite and pools of coarse-grained K-feldspar contain grains of sieve-textured

TABLE 2. COMPOSITION OF PHLOGOPITE FROM XENOLITHS AND LAMPROITES

sample location	1 T072-X3 rind 5	2 T218-X core&rind 16	3 T277-X2 core&rind 13	4 T195-X core 4	5 T195-X rind 3	6 T195-X secondary 6	7 A138 core&rind 5	8 average phenocryst 38	9 P310 gmass 7	10 hi Fe-Ti xenocryst 6
SiO <sub>2</sub>	39.75	41.53	41.86	38.81	39.00	39.26	40.49	39.71	44.83	36.79
TiO <sub>2</sub>	0.98	0.82	0.68	0.57	0.63	0.63	1.12	2.32	0.31	7.20
Al <sub>2</sub> O <sub>3</sub>	12.08	13.28	13.06	13.69	13.86	13.57	13.19	12.27	9.11	14.15
Cr <sub>2</sub> O <sub>3</sub>	1.54	0.99	0.60	2.07	2.08	1.98	1.12	0.17	0.31	0.02
FeO	10.35	5.89	3.87	3.20	3.76	3.47	4.46	8.14	10.65	14.50
MnO	0.17	0.02	0.01	0.00	0.05	0.02	0.06	0.10	0.12	0.05
NiO	0.12	NA	NA	0.28	0.29	0.25	0.19	NA	NA	0.09
MgO	19.69	24.03	26.44	24.37	24.43	24.66	24.84	21.23	20.89	13.49
CaO	0.00	0.13	0.06	0.00	0.00	0.01	0.01	0.03	0.09	0.04
Na <sub>2</sub> O	0.05	0.28	0.40	0.24	0.35	0.24	0.51	0.19	0.04	0.35
K <sub>2</sub> O	10.25	9.57	10.09	10.00	9.58	10.10	9.63	9.60	8.33	8.80
BaO	0.38	NA	NA	0.28	0.22	0.29	0.27	0.38	0.00	1.76
F	0.53	NA	NA	0.39	0.42	0.45	1.67	1.26	1.21	0.51
O=F	-0.22	NA	NA	-0.16	-0.18	-0.19	-0.70	-0.53	-0.51	-0.21
sum	95.65	96.54	97.05	93.74	94.47	94.73	96.86	94.87	95.08	97.54

Analysis 8 is average phenocryst analysis from CIF lamproites; analysis 9 is of Al-deficient groundmass mica coexisting with high-Ti amphibole (Table 4; analysis 10 from LeCheminant et al. (1987). n=number of analysis points, NA=not analyzed.

phlogopite (Fig. 5d). These segregations seem to have resulted from partial melting of the xenolith.

#### Amphibole

Amphibole in the CIF rocks (Table 4) can occur as primary interstitial or poikilitic grains, as in many lamproites, but is typically secondary after clinopyroxene and groundmass minerals. Primary amphibole is usually pleochroic yellow to violet-brown, whereas secondary amphibole is pleochroic in shades of green, lavender, and blue. Few data on primary amphiboles are available. Titanian richterite is associated with Al-deficient phlogopite in the groundmass of sample P310. A syenitic clast in the breccia P92/213 consists

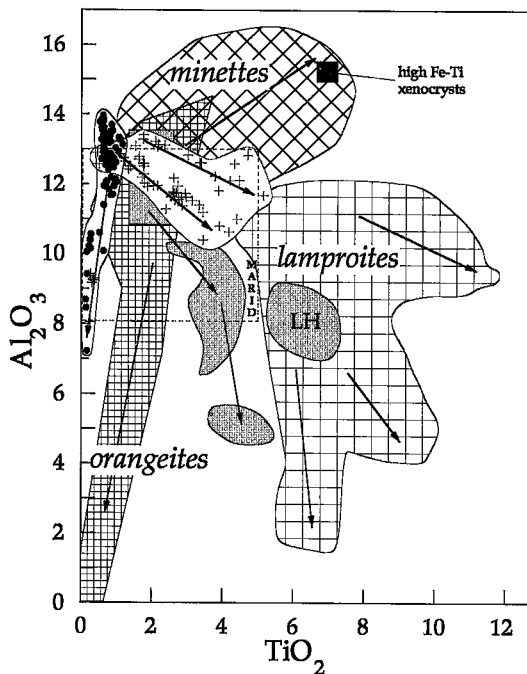


FIG. 6. Composition of phlogopite from glimmerite xenoliths (circles) and CIF lamproites (crosses) compared to that of phlogopite from other ultrapotassic rocks. The large square is the composition of a high-Fe-Ti-Ba xenocryst from a CIF dyke (Table 2). LH: Leucite Hills (box: phenocrysts; other: groundmass grains). Arrows indicate compositional trends from high-Mg to low-Mg micas. Fields from Mitchell & Bergman (1991).

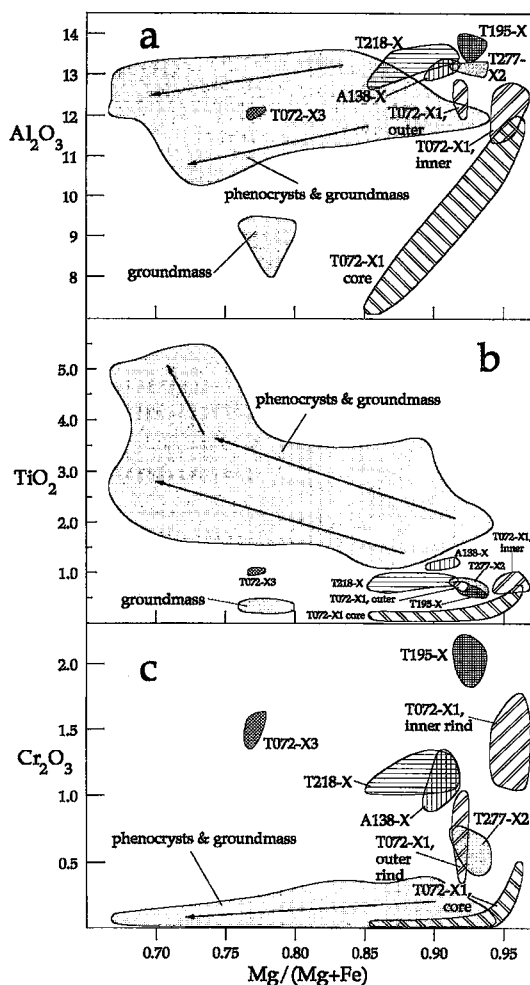


FIG. 7. a-c.  $\text{Al}_2\text{O}_3$ ,  $\text{TiO}_2$ , and  $\text{Cr}_2\text{O}_3$  versus  $\text{Mg}/(\text{Mg}+\text{Fe})$  for phlogopite phenocrysts and phlogopite from glimmerite xenoliths.

of sanidine laths ( $\text{Or}_{72}$ , Table 7) with interstitial and poikilitic titanian richterite; the sanidine is typical of lamproites (high Fe and Ba, and significant Ti), but both the sanidine and the titanian richterite are slightly less potassic than in most lamproites (Mitchell & Bergman 1991). The secondary amphibole replacing clinopyroxene is tremolitic; other secondary amphiboles are mainly solutions of richterite, winchite, and barroisite end-members. The amphibole (richterite – barroisite – kataphorite solid solution) associated with talc, dolomite, calcite, and resorbed phlogopite and chromian diopside in an angular xenolith from sample P310 contains 0.32%  $\text{Cr}_2\text{O}_3$ .

Zoned tremolitic and alkali amphiboles are common in the glimmerite xenoliths (Table 4). Xenolith T195 – X is the only one completely lacking amphibole. Xenoliths T072 – X1 and T072 – X2 contain

blades of colorless to pale blue and yellow pleochroic amphibole (K–Na-bearing richterite, winchite, and tremolite solid-solutions) that replaced phlogopite and chlorite in core calcite (Fig. 5b). Radiating bundles of secondary amphibole also project from the core–rind interface into the calcite. This amphibole has a lower molar  $\text{K}/(\text{Na}+\text{K})$  value (maximum 0.33) than is typical of MARID richterite and other examples of mantle richterite replacing phlogopite (range 0.44–0.47; Dawson 1987, Erlank *et al.* 1987). Equilibrium was not attained among the phlogopite, amphibole, and calcite; most of the amphibole is richteritic ( $\approx 5\%$  CaO), but that adjacent to calcite is more tremolitic [about 10% CaO, with  $\text{K}/(\text{Na}+\text{K}) \approx 0.11$ ]. In xenolith T072–X3, all calcite was consumed by reaction with phlogopite, and the cores of the xenoliths in dyke T072 are considered to preserve various stages in the reaction of the carbonate core with the phlogopite rind.

Xenolith T218–X contains colorless, coarse ( $\leq 2$  mm) tremolitic amphibole evenly distributed within the core and rind (Fig. 4a). In the core, the tremolite includes euhedral chromian epidote. Tremolite in the rind is present as both ribbon-shaped inclusions and equant, irregular grains concentrated along radial grain-boundaries in phlogopite.

#### Clinopyroxene

Clinopyroxene phenocrysts in the dykes and flows are colorless ferroan diopside (nomenclature of Morimoto 1989). Some have a Cr-enriched core ( $\leq 0.5\%$   $\text{Cr}_2\text{O}_3$ ) and a thin, bright green rim of ferroan sodian diopside. A pale green, partly resorbed core of ferroan sodian diopside is occasionally observed in the phenocrysts (LeCheminant *et al.* 1987), and it also occurs as discrete xenocrysts in the breccia P150. This paragenesis is identical to that of some Leucite Hills lamproites, as described by Barton & van Bergen (1981) and Mitchell & Bergman (1991).

The glimmerite clinopyroxene typically forms irregular grains of bright green chromian ferroan sodian diopside (Table 5), which are closely associated with chromite. Chromian diopside inclusions within high-Cr phlogopite xenocrysts are rarely euhedral (anal. 2, Table 5). The rind of xenolith T072–X2 is rich in broken and resorbed remnants of clinopyroxene that are optically continuous over distances up to 1 mm (Fig. 8). The grains are in some cases elongate parallel to the rind foliation, but never form the tapering ribbon-shaped inclusions typical of other phases. This pyroxene cannot be placed into any of the compositional ranges typical of garnet peridotites, garnet phlogopite peridotites, phlogopite peridotites, or MARID xenoliths (Erlank *et al.* 1987). It is exceptionally rich in Cr (3%  $\text{Cr}_2\text{O}_3$ ), Na (4%  $\text{Na}_2\text{O}$ ), and Fe (8% FeO) and has low Al ( $< 1\%$   $\text{Al}_2\text{O}_3$ ). Clinopyroxene in xenolith T072–X3 shows even more

TABLE 3. COMPOSITION OF PHLOGOPITE AND CHLORITE FROM XENOLITH T072-X1

location	1	2	3	4	5	6	7	8	9	10	11
n	2	2	2	3	2	2	2	2	2	2	3
SiO <sub>2</sub>	41.83	41.56	41.57	34.86	40.68	40.25	39.82	40.04	40.60	40.91	40.92
TiO <sub>2</sub>	0.26	0.69	0.17	0.04	0.72	0.71	0.75	0.77	0.76	0.72	0.72
Al <sub>2</sub> O <sub>3</sub>	10.38	11.93	8.62	11.82	12.36	12.65	12.69	12.76	12.43	12.36	12.10
Cr <sub>2</sub> O <sub>3</sub>	0.05	0.44	0.04	0.07	1.30	1.26	0.97	0.96	0.72	0.45	0.49
FeO	3.68	2.02	5.65	10.20	1.71	2.40	3.76	3.85	4.02	3.95	3.87
MnO	0.22	0.29	0.10	1.65	0.33	0.39	0.42	0.40	0.37	0.35	0.36
MnO	0.09	0.08	0.10	0.22	0.03	0.00	0.03	0.01	0.06	0.03	0.04
MgO	27.64	27.24	27.39	27.59	26.59	26.14	24.52	24.37	24.70	25.12	24.94
CaO	0.06	0.00	0.00	0.38	0.00	0.00	0.01	0.00	0.00	0.00	0.00
Na <sub>2</sub> O	0.11	0.12	0.05	0.02	0.09	0.11	0.12	0.11	0.11	0.08	0.06
K <sub>2</sub> O	10.27	10.30	10.35	0.16	10.42	10.07	10.26	10.32	10.30	10.50	10.33
BaO	0.26	0.09	0.16	0.08	0.36	0.36	0.31	0.36	0.32	0.34	0.35
F	0.92	0.85	0.77	0.46	0.96	0.78	0.87	0.77	0.92	0.83	0.78
O=F	-0.39	-0.36	-0.32	-0.19	-0.40	-0.33	-0.37	-0.32	-0.39	-0.35	-0.33
sum	95.34	95.22	94.68	87.36	94.13	94.77	94.14	94.36	94.88	95.27	94.60

Analyses 1-3 are of inclusions in the carbonate core; analysis 4 is average of chlorite replacing phlogopites #2 and #3. Analyses 5-11 are from a traverse from the inner rind towards the outer edge; locations are in mm from the inner boundary of the rind. n=number of analyses.

TABLE 4. COMPOSITION OF AMPHIBOLE FROM XENOLITHS AND LAMPROITES

sample location	1	2	3	4	5	6	7
n	6	11	3	5	6	2	6
SiO <sub>2</sub>	56.12	56.16	55.31	56.43	57.56	54.18	56.40
TiO <sub>2</sub>	1.51	0.13	0.08	0.08	0.09	3.07	5.14
Al <sub>2</sub> O <sub>3</sub>	1.56	0.30	0.30	0.39	0.87	2.31	0.87
Cr <sub>2</sub> O <sub>3</sub>	0.32	0.05	0.05	0.06	0.19	0.01	0.00
FeO	5.26	2.52	5.49	8.64	3.36	6.69	8.73
MnO	0.14	0.09	0.22	0.14	0.18	0.15	0.16
MgO	20.38	23.07	21.44	19.45	22.58	18.24	15.44
CaO	6.61	6.04	11.50	7.58	11.44	6.24	4.40
Na <sub>2</sub> O	6.10	4.54	1.74	3.43	1.37	5.82	5.85
K <sub>2</sub> O	1.19	2.76	0.67	1.71	0.52	1.36	2.07
BaO	0.03	0.04	0.01	0.01	0.05	0.11	0.04
F	1.76	0.86	0.41	0.43	0.39	1.20	1.71
O=F	-0.74	-0.36	-0.17	-0.18	-0.16	-0.51	-0.72
sum	100.22	96.23	97.05	98.17	98.42	98.93	100.12

Analyses #6 is from the groundmass of a lamproite flow; analysis #7 is of poikilitic amphibole including sanidine laths in a lamproite breccia fragment. n=number of analyses.

TABLE 5. COMPOSITION OF CLINOPYROXENE IN XENOLITHS AND LAMPROITES

sample location	1	2	3	4	5	6	7	8
n	6	9	6	3	8	7	4	3
SiO <sub>2</sub>	55.10	53.93	52.53	52.44	53.36	55.55	54.45	52.94
TiO <sub>2</sub>	0.24	0.13	0.31	1.07	0.53	0.12	0.16	0.44
Al <sub>2</sub> O <sub>3</sub>	0.89	0.78	0.34	0.34	1.53	0.31	0.45	0.52
Cr <sub>2</sub> O <sub>3</sub>	3.00	2.57	1.53	0.88	1.39	1.76	0.04	0.05
FeO	8.19	10.43	12.83	17.04	4.09	7.81	4.06	17.00
MnO	0.05	0.00	0.06	0.05	0.11	NA	0.05	0.04
MgO	0.07	0.16	0.32	0.31	0.08	0.18	0.11	0.21
CaO	10.90	9.75	9.08	6.07	16.34	13.75	17.53	8.00
Na <sub>2</sub> O	16.11	15.07	14.94	8.63	20.80	17.96	23.03	13.27
K <sub>2</sub> O	4.89	6.17	5.45	9.00	1.52	2.94	0.30	6.71
F	0.02	0.03	0.03	0.01	0.03	0.01	0.02	0.04
sum	99.50	99.03	97.42	95.85	99.79	100.40	100.18	99.21

Analysis #2 is of a euhedral inclusion in a disaggregated rind fragment. Analysis 4 is the average of three grains occurring with quartz, calcite, and rutile, and includes significant ZnO<sub>2</sub> and minor Cr<sub>2</sub>O<sub>3</sub>, Fe<sub>2</sub>O<sub>3</sub>, and V<sub>2</sub>O<sub>5</sub>. Analyses 7 and 8 are of the core and rind of a phenocryst in the lamproite matrix. n=number of analyses.

extreme compositions (>6% Na<sub>2</sub>O, >10% FeO). Anhedral clinopyroxene with about 1.4% Cr<sub>2</sub>O<sub>3</sub> and 1.5% Na<sub>2</sub>O is included in sieve-textured phlogopite in A138-X. This clinopyroxene has a composition intermediate between that typical of phlogopite - potassian richterite peridotites, and MARID xenoliths (Erlank *et al.* 1987).

Clinopyroxene in T277-X2 is olive green in color and has an unusual, non-quadrilateral composition. Pyroxene grains in rind interstices filled with quartz + euhedral rutile + carbonate have well-formed faces, are homogeneous and aegirine-rich (9% Na<sub>2</sub>O), enriched in TiO<sub>2</sub> (1%), and contain significant Zr, LREE, and possibly V (presence determined by energy-dispersion X-ray spectrometry). The analytical totals for these pyroxenes are low (95.9%).

### Spinel

The only spinel phase in the lamproites is low-Ti magnetite, occurring as phenocrysts and in the groundmass (Table 6). Chromite with high Cr/(Cr+Al) occurs as inclusions in phlogopite and clinopyroxene from several xenoliths of glimmerite, mainly as tiny (≤10 μm) euhedral grains in the rind. It also occurs as discrete, round xenocrysts less than 0.5 mm wide in the breccia P150. Trace quantities of low-Cr magnetite occur as trains of tiny (≤0.02 μm) irregular grains concentrated along the grain boundaries of core phlogopite in T218-X; this magnetite differs from groundmass magnetite in having high Cr/Al, Mn, and Zn. Concentrations of Zn and Mn are strongly correlated with Fe in all spinel grains from glimmerite. Relatively aluminous spinel occurs as euhedral grains

TABLE 6. COMPOSITION OF SPINELS IN LAMPROITE BRECCIA AND XENOLITHS

sample location	1	2	3	4	5	6	7	8	9	10	11	12
n	8	8	3	2	3	2	12	8	3	4	4	3
SiO <sub>2</sub>	0.26	0.12	0.13	0.16	0.18	0.09	0.12	0.25	0.07	0.08	0.12	0.73
TiO <sub>2</sub>	3.77	0.25	0.24	0.28	0.23	0.45	0.67	0.15	0.79	0.03	0.84	1.65
Al <sub>2</sub> O <sub>3</sub>	1.43	6.05	5.79	6.19	7.02	29.48	4.97	1.85	9.10	0.21	4.65	0.20
Cr <sub>2</sub> O <sub>3</sub>	0.05	62.80	61.85	57.53	57.25	27.77	56.61	54.05	51.48	8.34	35.34	3.32
FeO	84.24	13.12	16.63	24.19	22.93	23.93	25.82	32.97	28.26	80.41	40.46	85.15
NiO	0.08	0.29	0.21	0.14	0.17	0.29	0.07	0.05	0.10	0.33	0.34	0.07
MnO	0.13	0.22	0.33	1.85	1.69	0.36	0.90	3.53	0.79	0.53	5.35	0.20
MgO	1.05	15.71	13.23	7.13	8.52	12.66	6.55	0.65	6.26	0.04	0.18	0.43
CaO	0.09	0.01	0.04	0.04	0.06	NA	0.02	0.14	0.13	0.01	0.13	0.05
ZnO	0.00	0.07	0.07	0.25	0.15	0.26	1.19	2.11	1.21	0.65	5.38	0.19
V <sub>2</sub> O <sub>3</sub>	0.07	0.00	0.01	0.01	0.02	0.07	0.03	0.06	0.02	0.03	0.04	0.04
sum	91.16	98.63	98.53	97.74	98.22	95.34	96.96	95.80	98.22	90.65	92.82	92.03

Analysis 1 is of groundmass magnetite in lamproite breccia fragment; analyses 2, 3 are of discrete grains in breccia; analyses 4, 5 are of inclusions in phlogopite from disrupted glimmerites; analysis 12 is from a reaction rim around xenolith A138-X. n=number of analyses.

and clusters  $\leq 10 \mu\text{m}$  within high-Mg calcite in the core of xenolith T195-X. The spinel is concentrated near slightly resorbed phlogopite. This composition of spinel, which is typical of the early spinel in high-Mg lamproite (Mitchell & Bergman 1991), is only identified in T195-X. This xenolith also contains the most Cr-rich phlogopite in any of the glimmerite xenoliths.

The largest, most abundant, euhedral chromite grains ( $\leq 0.2 \text{ mm}$ ) are observed in the core of xenoliths T072-X1 and T072-X2, enclosed within calcite

and phlogopite (Fig. 9). Cr-Al zoning in these grains is patchy and extremely weak, but smooth zoning to a Fe-, Mn-, and Zn-rich rim is observed (atomic  $[\text{Mg}+\text{Ni}]/[\text{Mg}+\text{Ni}+\text{Fe}+\text{Mn}+\text{Zn}]$  in the range 0.33–0.28). Where in contact with phlogopite altered to high-(Mg, Ni) chlorite, the chromite has a diffuse alteration-related rim (not an overgrowth) containing Fe, Cr, and Si, with minor Ca and Mg.

Compositions listed in Table 6 are plotted in the spinel prisms in Figure 10. The Cr<sub>2</sub>O<sub>3</sub> content of the chromite ranges from 51% to 63% (excepting A138-X) and the atomic Mg/(Mg+Fe) ratio parallels that of coexisting clinopyroxene and phlogopite. The

TABLE 7. COMPOSITION OF MINERALS IN XENOLITHS AND BRECCIA

phase	1	2	3	4
sample location	calcite	epidote	titanite	sanidine
n	T072-X1	T218-X	T218-X	P92/213B
n	core	core	core	breccia
n	9	5	3	2
SiO <sub>2</sub>	NA	37.63	30.69	66.64
TiO <sub>2</sub>	NA	0.05	30.92	0.19
Al <sub>2</sub> O <sub>3</sub>	NA	21.83	4.22	17.46
Cr <sub>2</sub> O <sub>3</sub>	NA	0.49	0.18	0.00
FeO	0.04–1.59	12.77	1.85	1.14
NiO	NA	0.04	0.06	0.00
MnO	NA	0.12	0.04	0.00
MgO	0.27–4.25	0.15	0.04	0.02
CaO	46.4–58.19	21.97	28.02	0.01
Na <sub>2</sub> O	NA	0.03	0.00	3.00
K <sub>2</sub> O	NA	0.02	0.02	11.48
BaO	0–.16	0.00	0.04	0.99
SrO	0.17–1.14	NA	NA	NA
F	NA	0.00	1.60	0.00
OmF	NA	0.00	-0.68	0.00
sum	53–60	95.13	97.01	100.93

Analysis #1 is the observed range. Analysis #4 is sanidine associated with poikilitic amphibole in a syenite fragment. n=number of analysis points, NA=not analyzed.

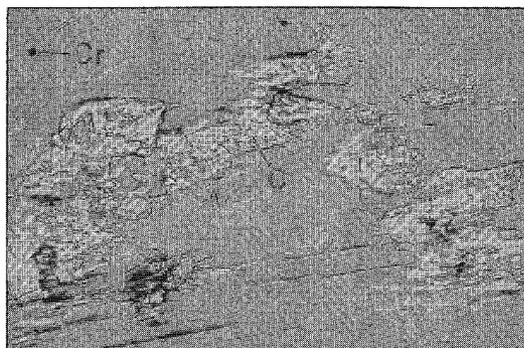


FIG. 8. Chromian diopside (C) in the rind of T072-X2. Cr: magnesiochromite (0.7 mm).

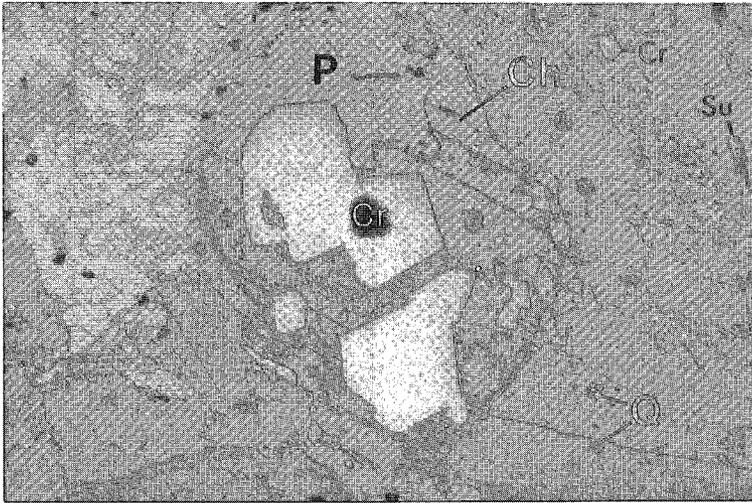


FIG. 9. Octahedra of chromite (Cr) in core phlogopite, T072-X1. Q: high-silica blebs in carbonate. Note the alteration fringe of high-Ni chlorite (Ch) around the phlogopite (P). Partly crossed polars (1.1 mm).

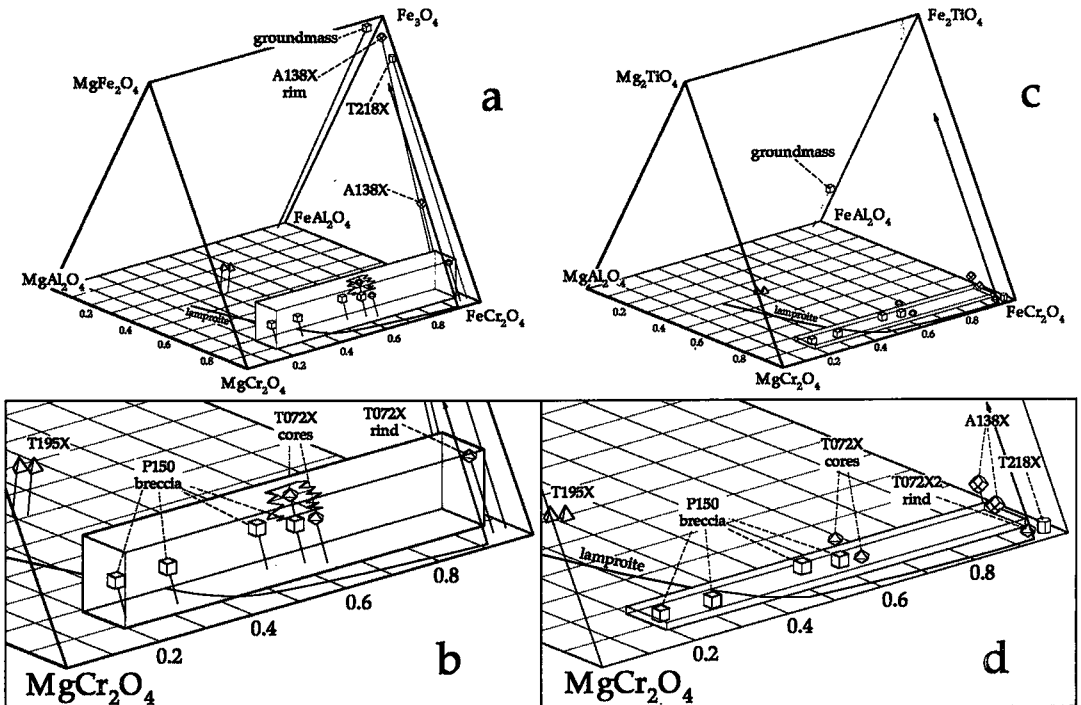


FIG. 10. Compositions of spinel. a, b. "Oxidized" prism. c, d. "Reduced" prism. The symbol labeled "groundmass" (sample P150) is the composition of microphenocrysts in the lamproite matrix; all others are from glimmerite xenoliths. The  $Fe_2O_4$ -rich spinel in A138-X is from the outer reaction rim; the other is an inclusion in phlogopite from the core. The rectangular boxes encompass the compositions of chromite occurring as inclusions in diamonds (data from Meyer & Boyd 1972, Gurney *et al.* 1979, Tsai & Meyer 1979, Gurney *et al.* 1984, Meyer 1987, Daniels & Gurney 1989). The curve marked "lamproite" is the compositional trend of spinel in lamproites (Mitchell & Bergman 1991).

most Mg-rich grains occur in breccia sample P150. Chromite in xenolith A138-X has only 35% Cr<sub>2</sub>O<sub>3</sub> and a high proportion of the Fe<sub>3</sub>O<sub>4</sub> component. Low-Cr magnetite in the reaction rim on the surface of this xenolith approaches the composition of magnetite in the groundmass.

The chromite from the glimmerite xenoliths has a composition typical of macrocrysts or early phenocrysts in lamproites and micaceous Group-I and Group-II kimberlites (orangeites), and closely approximates the lamproite trend of Mitchell & Bergman (1991). However, some of the chromite from the breccia P150 is more magnesian than this trend. Most of the chromite grains plot within a box defined by inclusions in diamond (the exception is chromite from the core of T072-X2, with slightly lower Cr/Al). The high-Fe end of this box is defined by inclusions in diamond from Sierra Leone (Meyer & Boyd 1972), which have high contents of Mn (0.43% MnO) and Zn (2.49% Zn), similar to the chromite from T072 xenoliths. (Fe, Zn)-rich chromite with a high Cr/(Cr+Al) value has also been found as inclusions in phlogopite in a lamproite dyke from Plan D'Albard, Italy (Wagner & Velde 1985).

#### *Carbonate minerals*

Calcite is the most abundant mineral in the glimmerite xenoliths after phlogopite. The core of xenoliths from the fine-grained portions of dyke T072 consists of calcite with lesser amounts of chromite, quartz, sulfides, titanite, phlogopite, amphibole, apatite, and

barite. Minor, irregular blebs of strontianite ( $\leq 50 \mu\text{m}$ ) also occur in the core, and one euhedral grain of strontianite was observed in the rind of T072-X1. The calcite (Table 7) is heterogeneous, with MgO  $\leq 4.25\%$ , FeO  $\leq 1.6\%$ , and SrO  $\leq 1.1\%$ . A single C-O isotope analysis of T072-X1 yielded a  $\delta^{18}\text{O}_{\text{SMOW}}$  of  $+5.53\%$ , and a  $\delta^{13}\text{C}_{\text{PDB}}$  of  $-7.36\%$ , at the light-C end of the mantle range (B. Kjarsgaard, pers. comm.).

In the core of xenolith T195-X, high-Mg calcite + quartz occur together as interstitial patches and round inclusions in the phlogopite. The patches, which are lined with calcite and contain quartz  $\pm$  chlorite in the center, are continuous with thin rims of carbonate that invade triple junctions among phlogopite grains, giving a strong impression of a melt phase (Fig. 5a). The phlogopite seems to have been nearly in equilibrium with this melt but is very slightly resorbed, and tiny euhedra of aluminous spinel within the calcite may have formed by incongruent melting of phlogopite. Irregular, secondary dolomite replaces phlogopite adjacent to calcite in the rind of this xenolith; unlike the calcite, it usually shows no morphological orientation relative to the basal cleavage of the mica host (Fig. 11).

#### *Epidote, titanite, zircon, apatite, and rutile*

Epidote (Table 7), varying from pale yellow to dark yellow-brown, is a common minor phase in xenoliths lacking chromite but relatively rich in tremolite, quartz, and titanite. Epidote in the core of xenoliths is palest in color. Epidote occurring as ribbon-shaped

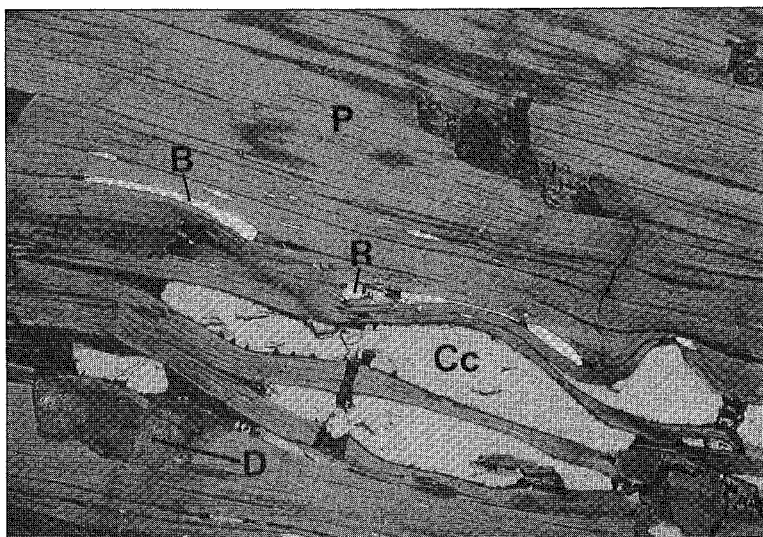


FIG. 11. Back-scattered electron image of the rind of T195-X, showing strongly deformed calcite (Cc) and barite (B) with broken grain of rutile (R). Dolomite (D) replaces phlogopite (P) and is not deformed (2.5 mm).

inclusions (Fig. 4a) is commonly more darkly colored and can be traced through to opaque blades consisting of fine-grained (<1  $\mu\text{m}$ ) calcite, magnetite, and quartz. The opaque blades are concentrated near the xenolith surfaces (and near quartz – calcite – rutile – pyroxene pools in T277–X2) and contain a folded internal foliation indicating shear parallel to the [001] plane of the host phlogopite. In T218–X, epidote is exceptionally abundant in both the rind and the core, where it occurs as irregular masses and as euhedral grains enclosed in tremolite.

Titanite (Table 7) is common in xenolith T218–X, where it occurs as slightly resorbed, subhedral grains ( $\leq 250 \mu\text{m}$ ) included in core phlogopite. Rare euhedral grains also were observed in the core of T072–X1. Subhedral zircon was only noted in the rind of xenolith T072–X3. A high-(U,Th,Pb) mineral (thorianite?) associated with an intense pleochroic halo also occurs in T072–X3 as tiny grains about 1  $\mu\text{m}$  across included in phlogopite. Apatite is a ubiquitous early phenocryst phase in the lamproites, but only rarely occurs in the glimmerite rinds. Rutile, a common late-stage groundmass mineral in the flows and dykes, is scarce in the xenoliths, but occurs as euhedral, partly metamict crystals in quartz–carbonate pools in T277–X2. It also occurs in T195–X as crystallographically oriented needles in core phlogopite, as tiny ( $\leq 5 \mu\text{m}$ ) round grains in carbonate, and as broken grains within the rind.

#### *Sulfides and sulfates*

The only sulfides detected are in xenoliths from dyke T072. Grains of Fe–Ni monosulfide occur along the grain boundaries of phlogopite in the inner portion of the rind, in association with chromite. Irregular masses of finely intermixed quartz and sulfides up to 100  $\mu\text{m}$  wide are included in calcite in the core. Partial rims of quartz may occur around the masses, and contiguous barite  $\pm$  goethite extends along the cleavage planes of the host carbonate. Si-free domains in the masses consist of pentlandite and pyrrhotite with round blebs of galena  $\leq 10 \mu\text{m}$  across. A partial electron-microprobe analysis yielded 27.1% Fe and 34.7% Ni, with S the only other detectable element (corresponding to  $\text{Fe}_{0.41}\text{Ni}_{0.50}\text{S}$ ). Galena also occurs as discrete, round grains  $\leq 10 \mu\text{m}$  across within calcite.

The silica-rich domains in the sulfide–silica masses are not homogeneous, but separate phases could not be resolved at a scale of about 1  $\mu\text{m}$ ; however, the sulfide in them is the same as in the silica-free domains. Minor As also was detected in the silica-rich domains. The textures of the silica–sulfide masses are consistent with liquid immiscibility, and can be ascribed to cooling of an impure sulfide melt that exsolved and coexisted with a silica-enriched liquid.

Ca–Ba sulfates occur within the core of T072–X3, and partly replace phlogopite in the core of T072–X1.

Minor ribbons of barite associated with calcite are present in the rind of T195–X.

#### *Quartz, feldspar and fluorite*

Quartz is abundant in the xenoliths, and commonly is associated with calcite. Most of the quartz occurs as ribbon-shaped inclusions within rind phlogopite. Some textures (*e.g.*, Fig. 4c) are consistent with precipitation between extending cleavage planes, but quartz in other ribbons has an undulatory extinction, indicating deformation. In T195–X, quartz, together with calcite, occurs as interstitial masses and round inclusions in core phlogopite. Small ( $\leq 100 \mu\text{m}$ ) inclusions of quartz + calcite in phlogopite from other xenoliths commonly contain acicular, pale blue alkali amphibole.

In T072–X1 and T072–X2, quartz forms a thin rim around the sulfide blebs and also numerous spherical polycrystalline globules  $\leq 10 \mu\text{m}$  across within the carbonate core (these also may be included in the sulfide blebs). Resorbed phlogopite in the core of these xenoliths contains large ribbons of quartz between cleavage planes; these are widest where phlogopite is replaced by chlorite.

K-feldspar commonly occurs in fractures and void spaces within ruptured phlogopite near xenolith surfaces and clearly was introduced from the magma. Irregular patches of K-feldspar occur within the micaceous segregations in xenolith A138–X, and within the reaction rim adjacent to the lamproite matrix. Fluorite occurs only in T218–X, where it forms irregular pools  $\leq 2 \mu\text{m}$  across in the core and scarce ribbon-shaped inclusions in the inner rind. The fluorite has patches that are vividly blue or purple.

### ORIGIN OF THE XENOLITHS

#### *Rind fabric*

The concentric rind of the xenoliths is an unusual feature and provides evidence for a complex dynamic history. Except for the calcite- and talc-cored xenoliths, the cores and rinds have very similar mineral assemblages and compositions, indicating formation under similar conditions. The rinds show clear evidence of deformation, including: (1) curvature of the [001] planes of individual phlogopite grains, (2) the presence of kink bands in phlogopite, (3) transposed fragments of optically continuous clinopyroxene, (4) folded inclusions, and “rolled-up” foliations in calcite–magnetite blades, and (5) boudinaged and ribbon-shaped inclusions indicating flattening perpendicular to [001] of phlogopite.

Kink-banding and bending of mica, and flattening of soft minerals (particularly ilmenite), are commonly observed in MARID xenoliths (Dawson 1987). The deformation textures of the glimmerite rinds can be

interpreted as due to repeated collisions with the conduit walls during ascent; other mechanisms, such as compaction in a magma chamber, are seemingly unable to account for the high symmetry of some of the xenoliths. We suggest that, upon impacting the wall, phlogopite either bent elastically, or (if the impact was sufficiently energetic) was kinked. The collisions shattered or flattened previously existing mineral inclusions, depending on their rheology (*e.g.*, clinopyroxene and rutile acted brittly, and calcite and quartz incompetently) and promoted precipitation of secondary minerals between cleavage planes as these dilated owing to slip on [001] surfaces.

The presence of secondary, nondeformed phlogopite cross-cutting the concentric rind foliation indicates that extensive recrystallization of deformed phlogopite occurred. The secondary mica is interpreted to have formed by annealing of the curvature of the xenolith rinds. Extensive annealing also may explain the excellent optical continuity of the best-formed rinds. Serrate grain-boundaries, concentrated in the tightest corners of the rinds, are probably recrystallized kink bands. Kink bands in phlogopite will migrate and recrystallize in a matter of hours at only 800°C and 3 kbar, resulting in a serrate grain-boundary (Etheridge & Hobbs 1974).

The predeformational state of the rinds is enigmatic because original textures have been destroyed. The presence of cores consisting of single grains of phlogopite with ribbon-shaped inclusions, which are continuous on one side with the rind, indicates that some xenoliths are folded fragments of disaggregated rinds, or are deformed megacrysts. Some of the xenoliths, particularly those with abrupt core-rind boundaries, may have originated as overgrowths of tangentially arranged phlogopite on phenocryst, xenocryst, or xenolith cores. For example, phlogopite overgrowths completely coat olivine and spinel cores in Leucite Hills lamproites (*cf.* Fig. 6.2 of Mitchell & Bergman 1991). Skjervaa (1992) interpreted the xenoliths of phlogopite-cored glimmerite from Oqaitsúnguit, Greenland, as the result of concentric growth around early phenocrysts of phlogopite. This is consistent with the normal zoning described in the phlogopite; however, some caution may be needed in this interpretation because those xenoliths are contained within a coarse-grained intrusion, and may have developed compositional gradients in the rind during slow cooling. Our xenoliths collected from quenched margins of dykes do not show any regular zoning, whereas those from coarse-grained centers of dykes display effects of considerable re-equilibration (*e.g.*, xenolith T072-X3). Abrasion of the surface, and extremely slow chemical diffusion perpendicular to [001] in phlogopite (Hofman *et al.* 1974), may have prevented the outer surface of the xenoliths from developing significant reaction rims or diffusion profiles.

The xenoliths of carbonate-cored glimmerite from

dyke T072 resemble spherical segregations in some carbonatites. Lapin & Vartiainen (1983) described examples of concentric growth of phlogopite surrounding carbonate-rich cores from Sökö, Finland and Vuorijärvi, Karelia. Numerous 1–3-cm nodules comprised of concentric layers of carbonate + phlogopite surrounding a sulfide- and calcite-rich core occur in the amphibole-rich margin of the lower Proterozoic Aley carbonatite, British Columbia (K. Pride, Cominco Exploration, pers. comm.).

The best-developed rinds have relatively flat sides and moderately curved corners; the cross-sectional shape varies from triangular (T277-X1, Fig. 2b) to quasi-elliptical. Xenolith T072-X1, in particular, has a very smooth, optically continuous rind with a cross-sectional shape closely approximating that of architect Piet Hein's "superellipses" (Gardner 1965), which have the formula  $(x/a)^n + (y/b)^n = 1$ , where  $n > 2$  (Fig. 3a). Superellipses have flattened sides and ends; a superellipse at the limit of  $n = \infty$  is a rectangle. For the xenoliths, this shape can be interpreted as a compromise between maintaining a flat [001] phlogopite surface with no lattice strain (rectangle), and a curved, concentric foliation arising from random impacts at the surface (ellipse). The three-dimensional form of a superellipse, called a superegg by Piet Hein, is closely approximated by several of the glimmerite xenoliths, leading to the field term "phlogopite superegg".

#### Primary mineralogy

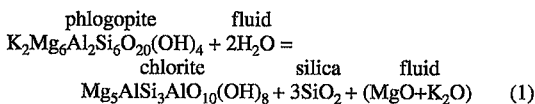
The P-T conditions of initial formation of the glimmerite xenoliths cannot be calculated, since appropriate mineral assemblages are not present. However, there can be little doubt that the xenoliths are mantle-derived, since they contain minerals typical of mantle peridotite and primitive melts, such as magnesiochromite, Ni-rich monosulfides, and chromian diopside. The high Mg, Cr, and Ni contents of the glimmerite xenoliths are consistent with precipitation from a high-K melt that interacted with (Cr,Ni)-rich mantle peridotites. Phlogopite, richterite, titanite, zircon, rutile, carbonate minerals, and chromian sodian diopside are commonly interpreted as metasomatic phases produced by interaction of silicate or carbonate melts, or C-H-O fluids, with mantle peridotite (*e.g.*, Erlank *et al.* 1987; Menzies *et al.* 1987).

The glimmerite xenoliths cannot be precipitates of the erupted lamproites since: (1) the phlogopite of the xenoliths is much lower in Ti, and higher in Al, Ni, and Cr, than the phenocrysts, and (2) mineral inclusions in the rind (chromite, chromian diopside) are not observed as phenocryst phases in the lamproites. However, phlogopite phenocrysts in the lamproites show a trend to lower Al, Cr, Ni, and higher Ti as Mg decreases. This is consistent with the hypothesis that the glimmerite xenoliths crystallized from ultrapotassic melts related to, but more primitive than, those

which ultimately carried the xenoliths to the surface. The paucity of Ti-rich phases in the glimmerite xenoliths mirrors the unusually low Ti contents of the CIF flows and dykes relative to most other ultrapotassic rocks (Peterson *et al.* 1993). Nd isotopic data (Esperança & LeCheminant 1986) also support a genetic association between the glimmerite xenoliths and the lamproites.

We interpret the glimmerite xenoliths to represent crystallized ultrapotassic melts, perhaps including some fragments of metasomatized or altered wallrocks coated with phlogopite. In particular, the talc-rich core of some xenoliths (*e.g.*, T277–X2) may represent altered peridotite. The high Cr content of amphibole associated with talc in P310–X is consistent with replacement of peridotite. Xenoliths A138–X and T195–X, which have a core of polycrystalline phlogopite, are interpreted to be cumulates formed from Cr-rich ultrapotassic melts with phlogopite  $\pm$  chromite  $\pm$  clinopyroxene on the liquidus.

The cores in xenoliths from dyke T072 indicate that carbonate-rich bodies were present in or above the source region. The igneous mineralogy and textures of these cores (*e.g.*, large, euhedral grains of normally zoned chromite) are inconsistent with deposition from a C–H–O fluid. There is no textural evidence that the carbonate replaced another phase (such as a clinopyroxene megacryst with phlogopite and chromite inclusions). Importantly, similar (Ti,Al)-poor phlogopite is associated with calcite in the groundmass of flow P310, suggesting an association between carbonate and low-Al phlogopite. Magnesiochromite is an unusual phase in carbonatites; however, it occurs in dolomitic carbonatite lapilli from southeastern Zambia, associated with K-rich silicate volcanism (Bailey 1989). We interpret the cores of xenoliths T072–X1 and T072–X2 to represent crystallized residual melts derived from a CO<sub>2</sub>-rich ultrapotassic magma, perhaps having formed initially as carbonate-rich veins within glimmerite dykes. The rinds of these xenoliths, which contain silicate minerals but few or no carbonate minerals, are interpreted as overgrowths of the phenocryst phases in the primitive ultrapotassic melt. Alteration of phlogopite in the core to chlorite + silica + other phases predated the formation of metamorphic amphibole (which replaced both phlogopite and chlorite) and probably occurred near the solidus of the vein material in the presence of an H<sub>2</sub>O-rich fluid or melt phase, *e.g.*,



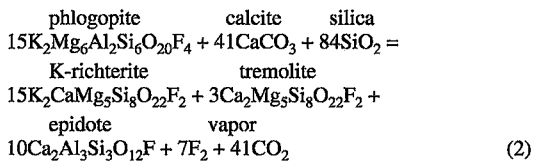
The compositional trend of late phlogopite in the carbonate-rich residua is fundamentally different than that in the lamproites, except where these are locally rich in calcite. This composition is not pressure-depen-

dent, since similar micas crystallizing at low pressure occur in the groundmass of orangeites.

#### *Re-equilibration, and secondary minerals*

Xenolith T072–X3 shows indications of mass exchange with the carrier magma. This xenolith, from a coarse-grained portion of the dyke, has a ragged, partly disaggregated rind, and contains relatively Fe-rich phlogopite, amphibole, and clinopyroxene. Xenolith A138–X, with clear indications of partial melting, contains relatively (Mg,Cr)-poor chromite in the interior, and Cr-rich magnetite in the outer reaction rim that approaches the groundmass magnetite in composition. The F content of phlogopite in A138–X is similar to that of the phenocrysts (Table 2), whereas phlogopite in the other xenoliths contains about half as much F. These observations indicate that (at least) Fe–Mg and F–OH exchange did occur between magma and strongly heated xenoliths.

The absence of amphibole in xenolith T195–X, and the presence of textures attributed to replacement in the other xenoliths, suggest that all amphibole formed by mineral reactions during ascent. Epidote is equally abundant, and exhibits similar textures, in several xenoliths. Both minerals can be written as products of reactions involving phlogopite, calcite, and a silica polymorph, such as:



with (OH) and H<sub>2</sub>O partly substituting for F and F<sub>2</sub>. Amphibole and epidote could have formed at the expense of phlogopite, calcite, and silica as a vapor phase escaped the xenolith during heating and decompression. The amphibole also contains significant Na that may have come from carbonate minerals, or from clinopyroxene, also replaced by tremolite. Reactions of this type are particularly applicable to xenolith T218–X, which contains fluorite that was probably produced by reaction between a Ca-rich phase and F produced by the breakdown of phlogopite.

The common presence of quartz in the xenoliths is unusual. The textures are inconsistent with post-igneous introduction of silica; we interpret the quartz as being either primary or secondary (metamorphic). The quartz occurring as ribbon-shaped inclusions in phlogopite may have been dissolved and reprecipitated as a consequence of deformation and is of uncertain origin. Xenolith T195–X, which shows the least amount of re-equilibration of any xenolith (*e.g.*, lack of amphibole and epidote, extremely homogeneous compositions of mica), clearly contained a melt phase in the core that crystallized to a silica polymorph +

impure calcite + other phases. This indicates that silica + calcite + phlogopite may have been a stable pre-entrapment assemblage in several xenoliths, with the carbonate- and silica-rich material remelting and migrating throughout the xenolith during ascent. Since an antipathetic relation is observed between clinopyroxene and calcite + silica, a reaction relation between clinopyroxene and melt to produce near-solidus carbonate and SiO<sub>2</sub> may have been in operation.

As is common for lamproites, the Keewatin ultrapotassic rocks have unusually high silica contents for rocks with high values of mg# and high contents of compatible trace elements. The glimmerite xenoliths indicate that siliceous ultrapotassic melts, or carbonate-rich residua from them, can be saturated with a silica phase at high pressure. Coesite has appeared as a subliquidus phase in experiments with a sanidine phlogopite lamproite from the Leucite Hills at 55–70 kbar (Mitchell 1992).

#### DISCUSSION

It has been suggested that MARID-suite xenoliths are fragments of chilled lamproite (Waters 1987) or possibly Group-II kimberlites (orangeites) (Mitchell & Bergman 1991), or are formed by a combination of igneous crystallization and metasomatism from kimberlites of an unspecified type (Kramers *et al.* 1983). The close analogy between spinel in the glimmerite xenoliths and that in micaceous kimberlites and lamproites suggests a genetic relation between the glimmerite xenoliths and lamproitic melts. The only example of magnesiochromite with high Cr/(Cr+Al) in minettes that is known to us occurs in Tertiary flows of the Bearpaw Mountains, Montana (MacDonald *et al.* 1992), in a region containing several young lamproitic centers.

Some petrologists interpret lamproites as partial melts of strongly metasomatized lithospheric mantle that was previously depleted by extraction of basaltic melts (*e.g.*, Venturelli *et al.* 1984). This sequence explains the strong depletion in Ca, Na, and Al, and enrichment in H, F, the LREE, and LILE seen in lamproites. The mineralogy of the glimmerite xenoliths is consistent with crystallization of a strongly ultrapotassic, even perpotassic, primitive melt depleted in Al and (especially) Ca, and rich in compatible and LIL elements. A plausible source-region for such a melt is metasomatized harzburgitic mantle. A more extensive discussion of the characteristics of the source region of the Keewatin lamproite magmas is to be found in Peterson *et al.* (1993).

The near-absence of Ti-bearing phases in the glimmerite is an unusual feature of this type of xenolith. This observation indicates that the strong depletion in Ti (and other HFSE) in the CIF relative to other lamproites and minettes is a characteristic of one or more contributing components in the source region, and of

the primary magmas of the CIF. Peterson *et al.* (1993) argued that a contemporaneous, subducted sediment component is strongly represented in the CIF. As indicated by results of Pb isotopic and trace-element analyses, sample T072, which contains very carbonate-rich xenoliths, contains an unusually large fraction of this component. Thus, some erupted CIF magmas probably originated in metasomatized mantle overlying an oceanic slab that was subducted shallowly beneath the central Churchill Province before 1.85 Ga (Peterson 1992). Near-contemporaneous subduction events can also be implicated in the genesis of other carbonate-rich lamproites, such as at Jumilla, Spain (Venturelli *et al.* 1991). Given the mineralogical and geochemical analogies of the CIF suite to minettes, lamproites, and orangeites, it is likely to occupy a central position in the debate regarding the nature of lamproitic magma in the future.

#### ACKNOWLEDGEMENTS

We thank B. Kjarsgaard for reviewing early versions of this paper. Laura Radburn assisted with SEM work, and John Stirling assisted with the electron-microprobe analyses. Formal reviews by J.C. Roddick, S. Bergman, and an anonymous reviewer greatly improved the manuscript.

#### REFERENCES

- BAILEY, D.K. (1989): Carbonate melt from the mantle in the volcanoes of south-east Zambia. *Nature* **338**, 415–418.
- BARTON, M. & VAN BERGEN, M.J. (1981): Green clinopyroxenes and associated phases in a potassium-rich lava from the Leucite Hills, Wyoming. *Contrib. Mineral. Petrol.* **77**, 101–114.
- BERGMAN, S.C. (1987): Lamproites and other potassium-rich igneous rocks: a review of their occurrence, mineralogy and geochemistry. In *Alkaline Igneous Rocks* (J.G. Fitton & B.G.J. Upton, eds.). *Blackwell, London* (103–190).
- BLAKE, D.H. (1980): Volcanic rocks of the Paleohelikian Dubawnt Group in the Baker Lake – Angikuni Lake area, District of Keewatin, N.W.T. *Geol. Surv. Can., Bull.* **309**.
- DANIELS, L.R.M. & GURNEY, J.J. (1989): The chemistry of the garnets, chromites and diamond inclusions of the Dokolwayo kimberlite, Kingdom of Swaziland. In *Kimberlites and Related Rocks* (J. Ross *et al.*, eds.). *Geol. Soc. Am., Spec. Publ.* **14**, 1012–1021.
- DAWSON, J.B. (1987): The MARID suite of xenoliths in kimberlite: relationship to veined and metasomatized peridotite xenoliths. In *Mantle Xenoliths* (F.R. Boyd, ed.). John Wiley and Sons, London (465–474).
- ERLANK, A.J., WATERS, F.G., HAWKESWORTH, C.J., HAGGERTY, S.E., ALLSOPP, H.L., RICKARD, R.S. & MENZIES, M.A. (1987): Evidence for mantle metasoma-

- tism in peridotite nodules from the Kimberley pipes, South Africa. In *Mantle Metasomatism* (M.A. Menzies & C.J. Hawkesworth, eds.). Academic Press, London (221-274).
- ESPERANÇA, S. & LECHEMINANT, A.N. (1986): Isotopic evidence for multiple enrichment events from mica-lamprophyre dykes in the District of Keewatin, Canada. *Geol. Soc. Am., Abstr. Programs* **18**, 595.
- ETHERIDGE, M.A. & HOBBS, B.E. (1974): Chemical and deformational controls on recrystallization of mica. *Contrib. Mineral. Petrol.* **43**, 111-124.
- GARDNER, M. (1965): The "superellipse": a curve that lies between the ellipse and the rectangle. *Sci. Am.* **213**, 222-230.
- GURNEY, J.J., HARRIS, J.W. & RICKARD, R.S. (1979): Silicate and oxide inclusions from the Finsch kimberlite pipe. In *Proc. Sec. Int. Kimberlite Conf.*, Vol. 1 (F.R. Boyd & H.O.A. Meyer, eds.). Am. Geophys. Union, Washington (1-15).
- , ——— & ——— (1984): Silicate and oxide mineral inclusions in diamonds from the Orapa mine, Botswana. In *Kimberlites II: The Mantle and Crust-Mantle Relationships* (J. Kornprobst, ed.). Elsevier, Amsterdam (25-34).
- HAGGERTY, S.E. (1989): Upper mantle opaque mineral stratigraphy and the genesis of metasomites and alkali-rich melts. In *Kimberlites and Related Rocks*, vol. 2 (J. Ross *et al.*, eds.). *Geol. Soc. Am., Spec. Publ.* **14**, 687-699.
- HOFMAN, A.W., GILETTI, B.J., HINTHORNE, J.R., ANDERSON, C.A. & COMAFORD, D. (1974): Ion microprobe analysis of a potassium self-diffusion experiment in biotite. *Earth Planet. Sci. Lett.* **24**, 48-52.
- HOFFMAN, P.F. (1980): Wopmay orogen: a Wilson cycle of Early Proterozoic age in the northwest of the Canadian Shield. In *The Continental Crust and its Mineral Deposits* (D.W. Strangway, ed.). *Geol. Assoc. Can., Spec. Pap.* **20**, 523-549.
- & PETERSON, T.D. (1991): Tectonic evolution of the Keewatin Hinterland during the consolidation of Laurentia (1.8-1.6 Ga). *Geol. Assoc. Can. - Mineral. Assoc. Can., Program Abstr.* **16**, A57.
- KRAMERS, J.D., RODDICK, J.C.M. & DAWSON, J.B. (1983): Trace element and isotope studies on veined, metasomatic and "MARID" xenoliths from Bultfontein, South Africa. *Earth Planet. Sci. Lett.* **65**, 90-106.
- LAPIN, A.V. & VARTIAINEN, H. (1983): Orbicular and spherulitic carbonatites from Sökli and Vuorijärvi. *Lithos* **16**, 53-60.
- LECHEMINANT, A.N., MILLER, A.R. & LECHEMINANT, G.M. (1987): Early Proterozoic alkaline igneous rocks, District of Keewatin, Canada: petrogenesis and mineralization. In *Geochemistry and Mineralization Proterozoic Volcanic Suites* (T.C. Pharoah *et al.*, eds.). *Geol. Soc. London, Spec. Publ.* **33**, 219-240.
- MACDONALD R., UPTON, B.G.J., COLLERSON, K.D., HEARN, B.C., Jr. & JAMES, D. (1992): Potassic mafic lavas of the Bearpaw Mountains, Montana: mineralogy, chemistry, and origin. *J. Petrol.* **33**, 305-346.
- MENZIES, M.A., ROGERS, N., TINDLE, A. & HAWKESWORTH, C.J. (1987): Metasomatic and enrichment processes in lithospheric peridotites, an effect of asthenosphere-lithosphere interaction. In *Mantle Metasomatism* (M.A. Menzies & C.J. Hawkesworth, eds.). Academic Press, London (313-364).
- MEYER, H.O.A. (1987): Inclusions in diamond. In *Mantle Xenoliths* (F.R. Boyd, ed.). John Wiley and Sons, London (501-522).
- & BOYD, F.R. (1972) Composition and origin of crystalline inclusions in natural diamonds. *Geochim. Cosmochim. Acta* **36**, 1255-1273.
- MITCHELL, R.H. (1985): A review of the mineralogy of lamproites. *Trans. Geol. Soc. S. Afr.* **88**, 411-437.
- (1992): High pressure experimental studies of sanidine phlogopite lamproite from the Leucite Hills, Wyoming. *Trans. Am. Geophys. Union (Eos)* **73**, 142 (abstr.).
- & BERGMAN, S.C. (1991): Lamproites. *Plenum Press, New York*.
- MORIMOTO, N. (1989): Nomenclature of pyroxenes. *Can. Mineral.* **27**, 143-156.
- NĚMEC, D. (1974): Petrochemistry of the dyke rocks of the Central Bohemian Pluton. *Neues Jahrb. Mineral. Monatsh.*, 193-209.
- PETERSON, T.D. (1992): Early Proterozoic ultrapotassic volcanism of the Keewatin Hinterland, Canada. In *Proc. 5th Int. Kimberlite Conf. Vol. 1. Kimberlites, Related Rocks and Mantle Xenoliths* (H.O.A. Meyer & O.H. Leonardos, eds.). Companhia de Pesquisa de Recursos Minerais (Brasília) (221-235).
- , ESPERANÇA, S. & LECHEMINANT, A.N. (1993): Geochemistry and origin of the ultrapotassic rocks of the District of Keewatin, Canada. *Mineral. Petrol.* (in press).
- SCOTT SMITH, B.H. (1989): Lamproites and kimberlites in India. *Neues Jahrb. Mineral. Abh.* **161**, 193-225.
- SKERJNAA, L. (1992): A lamproite stock with ellipsoidal phlogopite nodules at Oqaitšinguit, Disko Bugt, central West Greenland. *Rapp. Grønlands Geol. Unders.* **154**, 33-47.
- SMITH, H.G. (1936): New lamprophyres and monchiquites from Jersey. *Quart. J. Geol. Soc. London* **42**, 365-383.
- TELLA, S., HEYWOOD, W.W. & LOVERIDGE, W.D. (1985): A U-Pb age on zircon from a quartz syenite intrusion, Amer

- Lake area, District of Keewatin, NWT. *Geol. Surv. Can., Pap.* **85-1B**, 367-370.
- TSAI, H. & MEYER, H.O.A. (1979): Mineral inclusions in diamond: Premier, Jagersfontein, and Finsch kimberlites, South Africa, and Williamson Mine, Tanzania. In Proc. Second Int. Kimberlite Conf., Vol. 1 (F.R. Boyd & H.O.A. Meyer, eds.). Am. Geophys. Union, Washington, D.C. (16-26).
- VENTURELLI, G., THORPE, R.S., DAL PIAZ, G.V., DEL MORO, A. & POTTS, P.J. (1984): Petrogenesis of calc-alkaline, shoshonitic, and ultrapotassic Oligocene volcanic rocks from the northwestern Alps, Italy. *Contrib. Mineral. Petrol.* **86**, 209-220.
- VENTURELLI, S.C., BARBIERI, M., TOSCANI, L., MARIANA, E.S. & ZERBI, M. (1991): The Jumilla lamproite revisited: a petrological oddity. *Eur. J. Mineral.* **3**, 123-145.
- WAGNER, C. & VELDE, D. (1985): Mineralogy of two peralkaline, arfvedsonite-bearing minettes. A new occurrence of Zn-rich chromite. *Bull. Minéral.* **108**, 173-187.
- WATERS, F.G. (1987): A suggested origin of MARID xenoliths in kimberlites by high pressure crystallization of an ultrapotassic rock such as lamproite. *Contrib. Mineral. Petrol.* **95**, 523-533.

*Received July 8, 1992, revised manuscript accepted February 12, 1993.*